Order within disorder: The atomic structure of ion-beam sputtered amorphous tantala (a-Ta$_2$O$_5$)

Riccardo Bassiri, Franklin Liou, (iD) Matthew R. Abernathy, et al.

View Online   Export Citation   CrossMark

ARTICLES YOU MAY BE INTERESTED IN

Order within disorder: The atomic structure of ion-beam sputtered amorphous tantala (a-Ta$_2$O$_5$)

Riccardo Bassiri,[1,a] Franklin Liou,[1] Matthew R. Abernathy,[2] Angie C. Lin,[1]
Namjun Kim,[3] Apurva Mehta,[4] Badri Shyam,[4] Robert L. Byer,[1]
Eric K. Gustafson,[2] Martin Hart,[5] Ian MacLaren,[5] Iain W. Martin,[5]
Roger K. Route,[1] Sheila Rowan,[5] Jonathan F. Stebbins,[3]
and Martin M. Fejer[1]

[1]*E. L. Ginzton Laboratory, Stanford University, Stanford, California 94305, USA*
[2]*LIGO Laboratory, California Institute of Technology, Pasadena, California 91125, USA*
[3]*Department of Geological and Environmental Sciences, Stanford University, Stanford,
California 94305, USA*
[4]*Stanford Synchrotron Radiation Lightsource, SLAC National Accelerator Laboratory,
Menlo Park, California 94025, USA*
[5]*SUPA, School of Physics and Astronomy, University of Glasgow,
Glasgow G12 8QQ, United Kingdom*

Amorphous tantala (a-Ta$_2$O$_5$) is a technologically important material often used in high-performance coatings. Understanding this material at the atomic level provides a way to further improve performance. This work details extended X-ray absorption fine structure measurements of a-Ta$_2$O$_5$ coatings, where high-quality experimental data and theoretical fits have allowed a detailed interpretation of the nearest-neighbor distributions. It was found that the tantalum atom is surrounded by four shells of atoms in sequence; oxygen, tantalum, oxygen, and tantalum. A discussion is also included on how these models can be interpreted within the context of published crystalline Ta$_2$O$_5$ and other a-T$_2$O$_5$ studies. *© 2015 Author(s). All article content, except where otherwise noted, is licensed under a Creative Commons Attribution 3.0 Unported License.* [http://dx.doi.org/10.1063/1.4913586]

Amorphous heavy metal oxides are often used as the high refractive index layer of highly reflective dielectric thin film coatings. In particular, ion-beam sputtered (IBS) amorphous tantala (a-Ta$_2$O$_5$) is frequently used as the high index material of choice as it can exhibit relatively low levels of optical and mechanical loss. Applications that demand the high performance this coating material can often include optical atomic clocks,[1] ring laser gyroscopes,[2] frequency comb techniques,[3] and high-precision interferometers such as the Laser Interferometer Gravitational-wave Observatory (LIGO).[4] Amorphous tantala also has potential applications that include insulating films with high dielectric constant in electronics[5] and corrosion resistant coatings.[6]

To further improve the performance of these coatings, it has become necessary to understand changes in the material properties induced during the manufacturing process at the atomic level. For example, it has previously been shown that annealing and doping of these thin films can cause noticeable changes to both the optical loss and mechanical loss (internal friction).[7,8]

Recent work on this material suggests that changes in short-range order (SRO) (≤ 10 Å) strongly correlate with mechanical loss.[9] To better resolve such structural changes, we use Extended X-ray Absorption Fine Structure (EXAFS) measurements to probe the nearest neighbor distances from tantalum. Although amorphous materials do not exhibit long-range order characteristic of crystals, specific fragments with short-range order are still found throughout the material, making EXAFS a
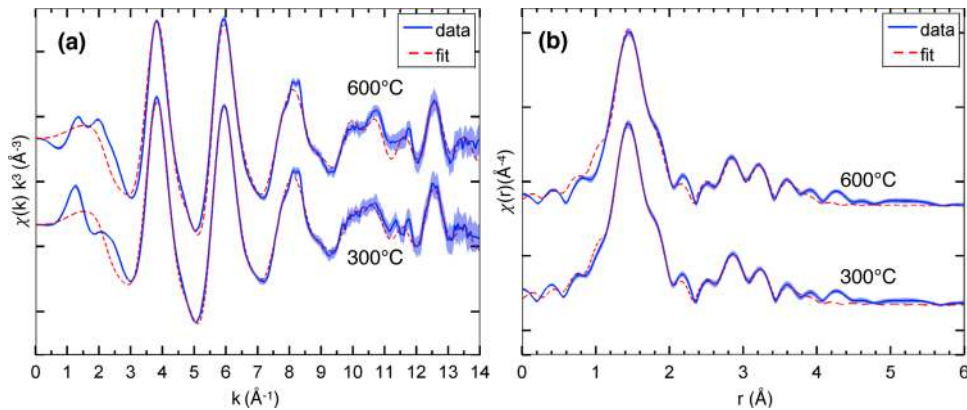
---

[a]Electronic mail: rbassiri@stanford.edu

FIG. 1. EXAFS (a) $\chi(k)$ spectra and (b) $\chi(r)$ spectra of the IBS amorphous tantala coatings annealed at 300 °C and 600 °C. The thickness of the data line represents the standard deviation of the data taken over several runs. The plots also include the FEFF fit lines.

useful tool for probing the atomic structure of amorphous materials such as the amorphous tantala studied in the current work.[10]

Results from Ta L_{III} EXAFS are presented here together with FEFF-based[11] fits to the data for IBS amorphous tantala annealed at 300 °C and 600 °C. These data are followed by a discussion of how this model can be interpreted with respect to previous studies of crystalline tantala.

The IBS amorphous tantala coating samples were manufactured by the Commonwealth Scientific and Industrial Research Organisation (CSIRO, Materials Science and Engineering Division, West Lindfield, NSW, Australia). The coatings were deposited onto fused silica substrates and were subject to post-deposition annealing at 300 °C and 600 °C for 24 h in air. Electron diffraction data show that both of these samples remained amorphous.[7]

The samples were characterized at beamline 4-3 at the Stanford Synchrotron Radiation Lightsource (SSRL). A standard experimental setup for collecting EXAFS was used, which allowed for simultaneous collection of the data at both fluorescence and transmission modes. The Ta L_{III} absorption edge has an energy of 9881 eV, and spectra were collected using a Lytle detector, with a Ni_6 filter, over an energy range 9700 eV–11020 eV. The data from the amorphous tantala were studied in both fluorescence and transmission; it was determined that self-absorption in fluorescence mode was negligible. Ultimately, fluorescence data for the coating were used for the analysis in this paper as it had a better signal-to-noise ratio than the transmission data.

In EXAFS spectra, information on the nearest neighbor distribution can be collected from the oscillatory part of the absorption coefficient above a major absorption edge, in this case Ta L_{III}, which is normally represented in k-space as the function, $\chi(k)$.[12] The EXAFS background subtraction and data extraction were carried out using the *Athena* data analysis package,[13] which includes background subtraction, alignment of the absorption energy, conversion to k-space, extraction of $\chi(k)$ data, and Fourier Transform (FT) to convert $\chi(k)$ to $\chi(r)$ components. Monochromator "glitches" in $\chi(k)$ were removed by directly deleting data points in the range of the glitch. The pre-edge and post-edge background was modeled as a third-order polynomial and the EXAFS region background as a polynomial spline. The k^3-weighted EXAFS $\chi(k)$ oscillations of the Ta L_{III} edge are shown in Fig. 1(a).

To represent this information in r-space, a Hanning FT window with a k-range of 3–14 Å^{-1}, slope parameter $dk = 1$, and a k^3-weighting was applied to $\chi(k)$ data, before taking the FT to obtain $\chi(r)$. The $\chi(r)$ data are shown in Fig. 1(b). The k-range was chosen to minimize the effect of low-energy multiple-scattering processes at low k and avoid the lower signal-to-noise data at high k.

Theoretical standards of the EXAFS oscillations were calculated by summing single scattering paths of the nearest neighbor atoms calculated via a self-consistent real space multiple-scattering approach as implemented in FEFF8.[11] The fitting parameters used were NS_0^2, the total scattering amplitude, where N is the co-ordination number and S_0^2 is the amplitude reduction factor; r, the

TABLE I. EXAFS fit parameters for IBS amorphous tantala annealed at 300 °C and 600 °C.

	300 °C				600 °C			
Path	r (Å)	σ^2 (Å^2)	NS_0^2	$N(S_0^2 = 0.8)$	r (Å)	σ^2 (Å^2)	NS_0^2	$N(S_0^2 = 0.8)$
Ta-O	1.85(4)	0.0024(27)	1.52(172)	1.90(216)	1.84(8)	0.0021(60)	1.26(350)	1.57(437)
Ta-O	1.99(6)	0.0058(57)	2.48(178)	3.11(223)	1.98(12)	0.0063(122)	2.54(369)	3.18(461)
Ta-Ta	3.14(2)	0.0075(25)	1.14(61)	1.42(76)	3.14(4)	0.0077(52)	1.11(115)	1.39(143)
Ta-O	3.55(2)	0.0024(24)	1.98(57)	2.47(72)	3.55(3)	0.0011(34)	1.82(90)	2.27(113)
Ta-Ta	3.88(3)	0.0066(68)	0.41(58)	0.52(73)	3.89(4)	0.0069(84)	0.65(109)	0.81(137)

distance to the neighboring atom; σ^2, the Mean Square Relative Displacement (MSRD); and E_0, the absorption energy. Since the value of S_0^2 is typically between 0.8 and 1.0, it is possible to obtain a lower and upper bound on N for each distinct scattering path.[14]

Fits were performed on $\chi(r)$ using IFEFFIT[15] with three free parameters per path plus an additional parameter for the absorption energy. Our fitting range for Δr and Δk are 1–4 Å and 3–14 Å^{-1}, respectively. The fitting results for all samples are listed in Table I. It was identified that a 4-shell model consisting of (in order of increasing distance from Ta) oxygen, tantalum, oxygen, and tantalum provides the best fit to the EXAFS spectra. The EXAFS $\mathcal{R}$-factor was used as a standard least-squares metric for the quality of fits,[12] with obtained values 0.004 and 0.011 for the samples annealed at 300 °C and 600 °C, respectively, indicating very good fits ($\mathcal{R} \leq 0.02$).[14] Since different Ta atoms in amorphous tantala can have a range of coordination numbers, the degeneracy of each path need not be an integer.

The atomic structure differences between 300 °C and 600 °C annealed temperatures identify only a subtle effect on the short-range order of the amorphous tantala samples, since all of the EXAFS fitting parameters for the two samples are within the error of one another as highlighted in Fig. 2. Since macroscopic properties are observed to change upon annealing,[7] the nature of the structural changes associated with annealing remains a subject of ongoing investigations. It has been observed that amorphous tantala has noticeable structural changes in the medium-range order ($5 < r < 40$ Å) when annealing temperature is varied.[16]
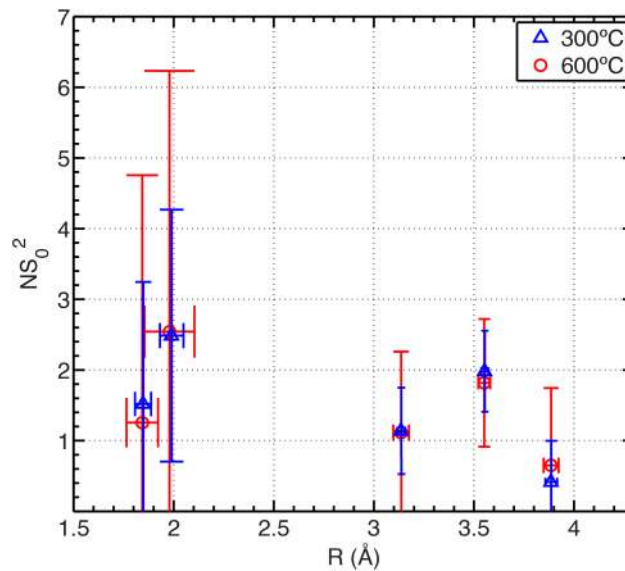

FIG. 2. EXAFS fitting parameters of total scattering amplitude, NS_0^2, plotted against nearest neighbor distances, r. It can be seen that changes in the short-range atomic structure of amorphous tantala with different annealing temperatures lie within the fitting uncertainties.
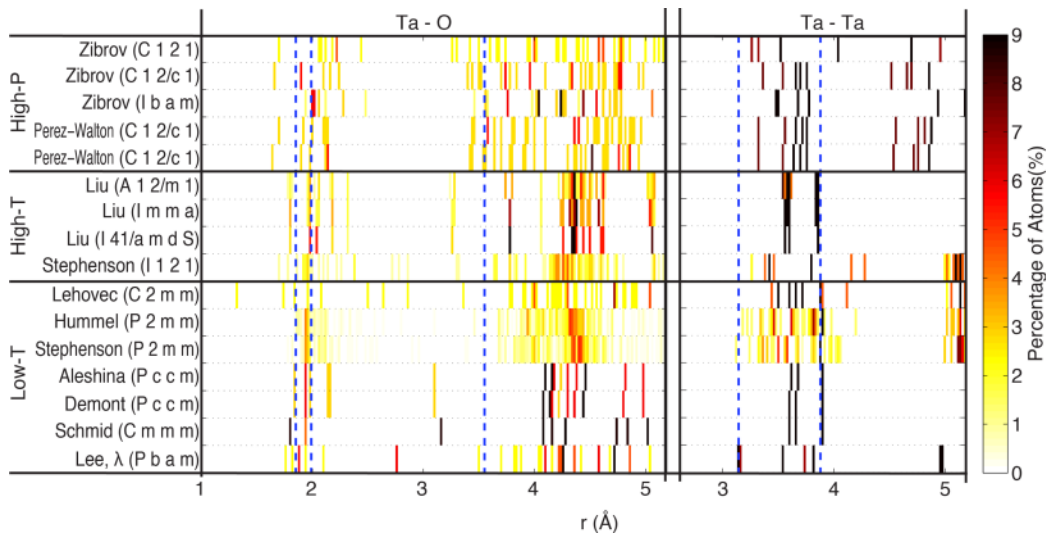
FIG. 3. Ta-O and Ta-Ta distance distributions of several crystalline tantala models.[17–28] The blue dashed lines represent the distances from the EXAFS fits of the amorphous tantala studied in this work.

The nearest neighbor distances obtained from the fits are compared with existing models of crystalline tantala in Fig. 3. The existence of oxygen at around 2 Å from a central tantalum agrees with typical chemical bond lengths. Our fits indicate that the first oxygen shell around tantalum consists of two distinct oxygen atoms at 1.85 and 2.0 Å, respectively, which appears to agree well with multiple models of the low-temperature phase of crystalline tantala, including the Aleshina and Demont models, belonging to space groups *Pccm*,[25,26] the Schmid, *Cmmm*,[27] and the Lee, λ model (space group *Pbam*).[28] In the former two models, the 1.85 Å oxygen is coordinated with two tantalum atoms and the 2.0 Å oxygen is coordinated with three tantalum atoms, which suggests that the two distinct Ta-O distances in amorphous tantala correspond to different oxygen sites. The first tantalum shell is at 3.1 Å, which agrees with the λ model.[28] The second Ta shell appears at 3.9 Å, which agrees with most models of crystalline tantala, except for high-pressure phase models. It is notable that the Ta shell at 3.5 Å present in several crystal models is absent in amorphous tantala. The fitted EXAFS distances are in good agreement with existing studies of amorphous tantala using electron diffraction[29] and EXAFS[30] for the first shell Ta-O distances, and provide a more detailed understanding of the metal-oxygen and metal-metal distances beyond 2 Å. The first shell also has potential correlations with a recent Nuclear Magnetic Resonance (NMR) spectroscopy study, which has shown the existence of two distinct types of oxygen sites, inferred to be 2 and 3-coordinated, respectively, in both amorphous and crystalline tantala.[31]

Since the amplitudes of the two oxygens in the first shell are strongly correlated with a correlation coefficient of −0.99, the errors on the individual amplitudes are large. However, the error on the total scattering amplitude (NS_0^2) of the first shell oxygens is substantially less, with 4.0 ± 0.22 and 3.8 ± 0.39 for samples annealed at 300 °C and 600 °C, respectively. With an S_0^2 of 0.8–1, the average coordination number of first-shell oxygens is 4–5. Compared to the published crystal structures, which have mostly 6 and 7-coordinated Ta, our fits indicate that Ta atoms in amorphous tantala have fewer neighboring oxygen atoms than those in crystalline tantala. The ^{17}O NMR data also suggest a lower mean Ta coordination in the amorphous phase than in the crystal, but with somewhat higher coordination numbers than are deduced from the EXAFS results, 6.5 and 6.0 for crystalline and IBS thin film samples, respectively.[31] Furthermore, the coordination numbers inferred from the EXAFS data are consistent with recent studies indicating a lower coordination in amorphous oxides and melts compared to their crystalline counterparts.[32–35] Further analysis of the first shell oxygen using non-parametric EXAFS fitting may reduce the associated uncertainty in the FEFF fitting by providing greater resolution,[36] and would be an interesting path for future investigations.

The σ^2 or MSRD parameter describes the sum of enthalpic and entropic disorders. Given that the two samples were measured at the same temperature, we can assume that changes in the

MSRD value reflect entropic disorder, i.e., spread in nearest neighbor distances. It was observed that the scattering paths involving the same scatterers tend to have similar MSRDs, and that tantalum scatterers have a larger MSRD than oxygen scatterers. A possible explanation for this phenomenon is valence disorder. If a central Ta atom can be either four or five-coordinated, the Ta-Ta distances can also depend on the coordination number of the central Ta atom. However, unlike the two and three-coordinated oxygen which can be fitted with only two absorber-scatterer distances, Ta-Ta distances also depend on the Ta-coordination number of the oxygen connecting them. This effect is reflected in a wider spread in Ta-Ta distance distributions, and thus a larger MSRD.

To summarize, we have analyzed high-quality EXAFS spectra of IBS amorphous tantala, annealed at 300 °C and 600 °C, and obtained high-quality fits based on single scatterers. The nearest neighbor distances were determined, as well as MSRDs and bounds on the average number of nearest neighbor atoms. The amorphous structures of tantala obtained consists of four shells of atoms, in sequence: oxygen, tantalum, oxygen, and tantalum, and it was possible to resolve two distinct oxygen distances within the first shell. Overall, the comparisons with the published crystalline structures show that amorphous tantala is not a simple distortion of a crystalline structure. Although the first shell fits in well with most of the published crystalline structures, our results suggest that there is significant rearrangement of the structural motif beyond 2 Å with some missing shells and the occurrence of the 3.1 Å Ta-Ta distance, which is only present in the λ crystalline model.

Future work will involve combining EXAFS data with other experimental measurements, and further exploration of the observed similarities to previous NMR and TEM studies. It will also be useful to combine the EXAFS data with electron and X-ray pair-distribution function analysis to study medium-range order structural difference. In addition, X-ray absorption near edge spectroscopy (XANES) may also provide additional insights into the coordination and electronic structure.[37,38] We anticipate that these studies will lead to further understanding of the changes induced in the coating atomic structure during common IBS coating manufacturing processes, such as annealing and doping, and stimulate further study into correlations with optical and mechanical losses.

[1] Y. Y. Jiang, A. D. Ludlow, N. D. Lemke, R. W. Fox, J. A. Sherman, L. S. Ma, and C. W. Oates, Nat. Photonics **5**, 158–161 (2011).
[2] D. A. Andrews, S. Roden, and T. A. King, IEEE J. Quantum Electron. **31**, 1709–1715 (1995).
[3] K. Numata, A. Kemery, and J. Camp, Phys. Rev. Lett. **93**, 250602 (2004).
[4] G. M. Harry and the LIGO Scientific Collaboration, Classical Quantum Gravity **27**, 084006 (2010).
[5] S. Zaima, T. Furuta, Y. Koide, Y. Yasuda, and M. Iida, J. Electrochem. Soc. **137**, 2876–2879 (1990).
[6] Y. L. Zhou, M. Niinomi, T. Akahori, H. Fukui, and H. Toda, Mater. Sci. Eng., A **398**, 28–36 (2005).
[7] I. W. Martin, R. Bassiri, R. Nawrodt, M. M. Fejer, A. Gretarsson, E. Gustafson, G. Harry, J. Hough, I. MacLaren, S. Penn, S. Reid, R. Route, S. Rowan, C. Schwarz, P. Seidel, J. Scott, and A. L. Woodcraft, Classical Quantum Gravity **27**, 225020 (2010).
[8] G. M. Harry, M. R. Abernathy, A. E. Becerra-Toledo, H. Armandula, E. Black, K. Dooley, M. Eichenfield, C. Nwabugwu, A. Villar, D. R. M. Crooks, G. Cagnoli, J. Hough, C. R. How, I. MacLaren, P. Murray, S. Reid, S. Rowan, P. H. Sneddon, M. M. Fejer, R. Route, S. D. Penn, P. Ganau, J.-M. Mackowski, C. Michel, L. Pinard, and A. Remillieux, Classical Quantum Gravity **24**, 405 (2007).
[9] R. Bassiri, K. Evans, K. B. Borisenko, M. M. Fejer, J. Hough, I. MacLaren, I. W. Martin, R. K. Route, and S. Rowan, Acta Mater. **61**, 1070–1077 (2013).
[10] E. E. Doomes and S. C. McGuire, Nucl. Instrum. Methods Phys. Res., Sect. A **582**, 245–247 (2007), Proceedings of the 14th National Conference on Synchrotron Radiation Research {SRI} 2007.
[11] A. L. Ankudinov, B. Ravel, J. J. Rehr, and S. D. Conradson, Phys. Rev. B **58**, 7565 (1998).
[12] M. Newville, Rev. Mineral. Geochem. **78**, 33–74 (2014).
[13] B. Ravel and M. Newville, J. Synchrotron Radiat. **12**, 537–541 (2005).
[14] S. Calvin, E. E. Carpenter, B. Ravel, V. G. Harris, and S. A. Morrison, Phys. Rev. B **66**, 224405 (2002).

[15] M. Newville, J. Synchrotron Radiat. **8**, 322–324 (2001).

[16] R. Bassiri, M. Hart, R. L. Byer, K. B. Borisenko, K. Evans, M. M. Fejer, A. C. Lin, I. MacLaren, A. S. Markosyan, I. W. Martin, R. K. Route, and S. Rowan, J. Phys.: Conf. Ser. **522**, 012043 (2014).

[17] I. P. Zibrov, V. P. Filonenko, M. Sundberg, and P.-E. Werner, Acta Crystallogr. B **56**, 659–665 (2000).

[18] I. P. Zibrov, V. P. Filonenko, D. V. Drobot, and E. E. Nikishina, Russ. J. Inorg. Chem+ **48**, 464–471 (2003).

[19] S. Pérez-Walton, C. Valencia-Balvín, G. M. Dalpian, and J. M. Osorio-Guillén, Phys. Status Solidi B **250**, 1644–1650 (2013).

[20] X. Q. Liu, X. D. Han, Z. Zhang, L. F. Ji, and Y. J. Jiang, Appl. Phys. Lett. **90**, 211904 (2007).

[21] N. C. Stephenson and R. S. Roth, J. Solid State Chem. **3**, 145–153 (1971).

[22] K. Lehovec, J. Less-Common Met. **7**, 397–410 (1964).

[23] H.-U. Hummel, R. Fackler, and P. Remmert, Chem. Ber. **125**, 551–556 (1992).

[24] N. C. Stephenson and R. S. Roth, Acta Crystallogr. B **27**, 1037–1044 (1971).

[25] L. A. Aleshina and S. V. Loginova, Crystallogr. Rep. **47**, 415–419 (2002).

[26] A. Demont, C. Prestipino, O. Hernandez, E. Elkaïm, S. Paofai, N. Naumov, B. Fontaine, R. Gautier, and S. Cordier, Chem. - Eur. J. **19**, 12711–12719 (2013).

[27] S. Schmid and V. Fung, Aust. J. Chem. **65**, 851 (2012).

[28] S.-H. Lee, J. Kim, S.-J. Kim, S. Kim, and G.-S. Park, Phys. Rev. Lett. **110**, 235502 (2013).

[29] R. Bassiri, K. B. Borisenko, D. J. H. Cockayne, J. Hough, I. MacLaren, and S. Rowan, Appl. Phys. Lett. **98**, 031904 (2011).

[30] D. Pickup, G. Mountjoy, M. Holland, G. Wallidge, R. Newport, and M. Smith, J. Mater. Chem. **10**, 1887–1894 (2000).

[31] N. Kim and J. F. Stebbins, J. Non-Cryst. Solids **378**, 158–162 (2013).

[32] L. B. Skinner, C. J. Benmore, J. K. R. Weber, J. Du, J. Neuefeind, S. K. Tumber, and J. B. Parise, Phys. Rev. Lett. **112**, 157801 (2014).

[33] N. Kim, R. Bassiri, M. M. Fejer, and J. F. Stebbins, J. Non-Cryst. Solids **405**, 1–6 (2014).

[34] D. B. Buchholz, Q. Ma, D. Alducin, A. Ponce, M. Jose-Yacaman, R. Khanal, J. E. Medvedeva, and R. P. H. Chang, Chem. Mater. **26**, 5401–5411 (2014).

[35] L. B. Skinner, A. C. Barnes, P. S. Salmon, L. Hennet, H. E. Fischer, C. J. Benmore, S. Kohara, J. K. R. Weber, A. Bytchkov, M. C. Wilding, J. B. Parise, T. O. Farmer, I. Pozdnyakova, S. K. Tumber, and K. Ohara, Phys. Rev. B **87**, 024201 (2013).

[36] D. S. Yang and G. Bunker, Phys. Rev. B **54**, 3169 (1996).

[37] S.-M. Paek and Y.-I. Kim, J. Alloy. Compd. **587**, 251–254 (2014).

[38] H. Asakura, T. Shishido, S. Yamazoe, K. Teramura, and T. Tanaka, J. Phys. Chem. C **115**, 23653–23663 (2011).